Journal of Bone Oncology 19 (2019) 100269

Contents lists available at ScienceDirect

Journal of Bone Oncology

journal homepage: www.elsevier.com/locate/jbo

Research Paper

Evaluating the scope of intramedullary invasion of malignant bone tumor by DCE-MRI quantitative parameters in an animal study

Zhang Yuan[a,b], Tan Yiqing[a], Dong Cheng[b], Gao Sai[b], Xu Wenjian[b], Chen Haisong[b,*]

[a] Department of Radiology, Wuhan Third Hospital (Tongren Hospital of Wuhan University), Wuhan, 430000, Hubei, China
[b] Department of Radiology, the Affiliated Hospital of Qingdao University, Qingdao 266003, China

ARTICLE INFO

Keywords:
VX2 tumor
Dynamic contrast enhancement magnetic resonance imaging (DCE-MRI)
Intramedullary invasion
Micro-infiltration

ABSTRACT

The purpose was to analyze the value of quantitative parameters of DCE-MRI in evaluating micro-infiltration of malignant bone tumors.

Methods: Thirty-nine New Zealand white rabbits were used to establish malignant bone tumor models by implanting VX2 tumor fragments into the right tibiae. After three weeks, models were examined by conventional MRI and DCE-MRI; then the right tibiae were cut into sagittal sections and partitioned into histology slices for comparison with microscopic findings. Micro-infiltration groups were selected and the range of infiltration was determined under the microscope, and corresponding DCE images analyzed to obtain the quantitative parameters include *Ktrans, Kep,* v_e and v_p in parenchyma areas, micro-infiltration areas and simple edema areas. One-way ANOVA was used to compare the differences of the parameters between the three areas. Receiver operating characteristic curves (ROCs) were plotted to determine the accuracy of different parameters by area under curves (AUCs).

Results: 22 cases (22/39, 56.4%) were included in the micro-infiltration group and the infiltration depth ranged from 1.3 mm to 4.6 mm, with an average depth of 3.2 mm ± 0.8 mm. The statistical results of quantitative parameters in the three areas were as follows: *Ktrans* values were (0.494 ± 0.052), (0.403 ± 0.049), (0.173 ± 0.047) min^{-1} ($p = =0.000$), *Kep* values were (1.959 ± 0.65), (1.528 ± 0.372), (1.174 ± 0.486) min^{-1} ($p = =0.000$), v_e values were (0.247 ± 0.068), (0.283 ± 0.057), (0.168 ± 0.062) min^{-1} ($p = =0.000$), v_p values were (0.125 ± 0.036), (0.108 ± 0.033), (0.098 ± 0.025) min^{-1} ($p = =0.022$), respectively. *Ktrans* and *Kep* values had significant difference in the three areas after comparing between-groups, respectively. However, there were no significant difference in v_p values between parenchyma and micro-infiltration areas ($p = =0.078$), micro-infiltration and simple edema areas ($p = =0.315$), and v_e values between parenchyma and micro-infiltration areas ($p = =0.056$). The v_e values were higher in parenchyma and micro-infiltration areas then simple edema areas. *Ktrans* had highest accuracy in differentiating different areas (AUC > 0.9), respectively.

Conclusion: Quantitative parameters *Ktrans, Kep* and v_e can assess the extent of intramedullary invasion of malignant bone tumors. *Ktrans* have highest accuracy in differentiating different regions.

1. Introduction

Definition of the surgical boundary of a bone tumor is the key to limb salvage surgery. However, the boundary of malignant bone tumors is often unclear, and conventional MR imaging could not accurately determine the depth of tumor invasion. In our previous study, computed tomography spectral curves and apparent diffusion coefficient values were used to distinguish the micro-infiltration area from simple edema area, the results showed the two methods were valuable [1–3], but both of the two examinations could not measure the microcirculation environment in different regions quantitatively.

T1-weighted dynamic contrast-enhanced magnetic resonance imaging (DCE-MRI) is a non-invasive technique which can provide quantitative information about tumor microcirculation environment [4,5]. Applications of DCE-MRI in musculoskeletal system include the assessment of tumors for characterization, treatment response after neoadjuvant therapy, and detection of recurrent after surgery [6,7]. Previous studies showed that DCE-MRI could aid in differentiating

Abbreviations: DCE-MRI, dynamic contrast-enhanced magnetic resonance imaging; ROC, receiver operating characteristic curve; AUC, area under curve

* Corresponding author.
E-mail address: abluesky12345@163.com (H. Chen).

https://doi.org/10.1016/j.jbo.2019.100269
Received 22 August 2019; Received in revised form 14 November 2019; Accepted 16 November 2019
Available online 20 November 2019

normal bone marrow from malignant infiltration [8–14]. However, an imaging method for distinguishing different areas, which could be useful for surgery of bone tumors has not been established. The purpose of this study was to analyze the value of quantitative parameters of DCE-MRI in evaluating micro-infiltration and differentiating different areas of malignant bone tumors.

2. Material and methods

2.1. Model preparation

The study was carried out in accordance with the EU Directive 2010/63/EU for animal experiments, and the ethics committee of the hospital where the study took place approved the research. Malignant bone tumor models were established as described in our previous study [1–3], using pure-bred male New Zealand white rabbits purchased from Qingdao Food and Drug Administration and weighing from 2.0 kg to 3.0 kg. The tumor was cut from the tumor-bearing rabbits and smashed into small fragments and implanted into the proximal part of right tibia of healthy rabbits with electrical drill and forceps. Then the bone defect was sealed with wax, the muscle and skin at the site of incision were sutured. Ketamine was injected into thigh muscles before the operation with a dose of 1.6 ml/kg.

2.2. Imaging examination

Imaging was performed three weeks after tumor implantation. MR imaging was performed on a Signa 3.0T MR scanner (General Electric Healthcare, Milwaukee, USA) using an 8-channel rabbit coil (Suzhou Zhongzhi Medical Technology Co., Ltd.). Protocols include pre-contrast axial, sagittal and coronal T1-weighted spin-echo sequences (TR/TE, 820/9.369; Fov, 20 cm; Nex 4), pre-contrast sagittal T2-weighted fast spin echo sequences (TR = 2940msec, TE = 85.816msec; Fov = 20 cm; Nex = 4), sagittal short time inversion recovery (STIR) sequences (TR = 3800 msec, TE = 38.92 msec; Inversion time = 180 msec; Fov = 20 cm; Nex = 4), with slice thickness 3 mm and interval 1 mm. Pre- and post-contrast sagittal fast spoiled gradient recalled echo sequences (TR = 6.5 msec, TE = 1.4 msec; Fov = 20 cm; Nex = 1; Matrix = 192 × 168; Slice thickness = 3 mm; Interval = 1 mm; Flip angle = 12°) were performed. Fifty phases were scanned. After the second phases, 1 ml/kg Gd-DTPA (Magnevist; Bayer Schering Pharma AG, Berlin, Germany) was administered followed by 10 ml saline flush injected at a rate of 1.5 ml/s with an automated injector. Pre-contrast T1 mapping images with multiple flip angles (8°,10°,12°) were obtained.

After scanning, data were transferred automatically to the workstation. Omni Kinetics software was used to quantitatively analysis. The femoral artery was manually labeled as the input artery.

2.3. Pathologic examination

After examination, the models were sacrificed by intravenous injection of air through the ear vein. The tibial specimens were immersed in formalin and preserved in a refrigerator at a temperature of −80 °C. Three days later, the specimens were cross-sectioned into sagittal plane and the layer thickness was 2 mm. The central section of the tumor was selected to compare with the corresponding sagittal MR image (Fig. 1A). The piece of the tissue that include half tumor (distal end) and half marrow were sectioned for hematoxylin-eosin staining (Fig. 1B).

Microscopic evaluation was performed to identify the relationships between the distal end of the tumor and bone marrow and to select the micro-infiltration group. The location of parenchyma area, micro-infiltration area and simple edema area were determined. The transition width of micro-infiltration was defined as the vertical distance between the tumor margin to the most distal tumor cells on the marrow side

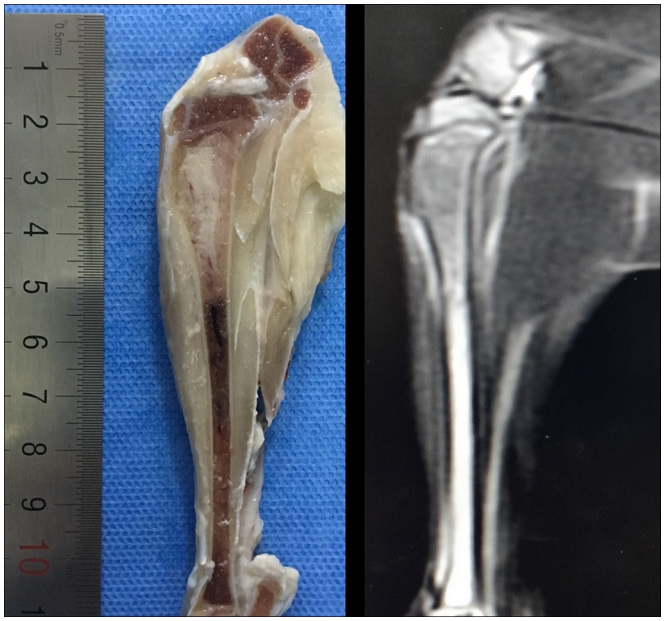

Fig. 1. (A) Maximal sagittal section of the specimen with a slice thickness of 2 mm and the corresponding magnetic resonance image of T2WI. **(B)** The figure shows the method for partitioning specimens and the corresponding magnetic resonance images. The location of the distal ends of the tumor in magnetic resonance images was determined using microscopy by the distance between distal tumors to the metaphysis (d), white line). The piece that include half tumor and half marrow (h-m, between the two orange lines) was sectioned for hematoxylin and eosin staining.

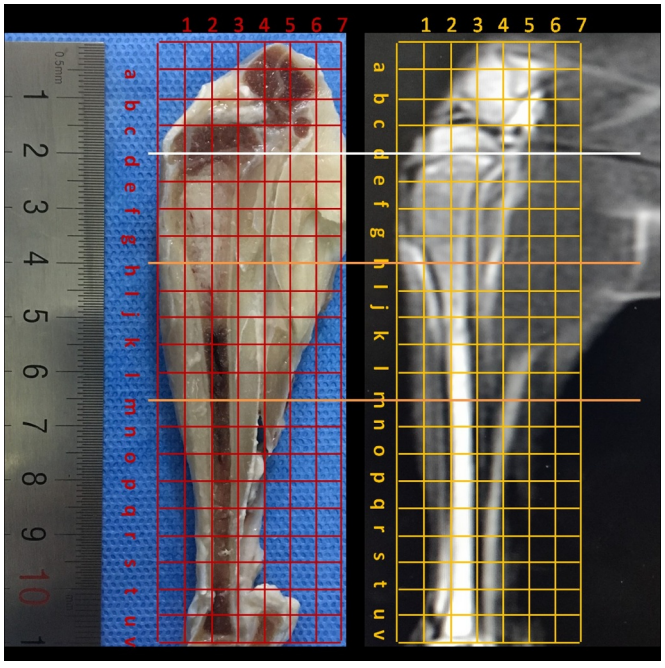

Fig. 1. (*continued*)

(Fig. 2) and measured by microscopy. The distance between the distal end to the proximal metaphysis of tibia was also detected and measured by microscopy. Experienced orthopedic pathologists examined all histological slides.

2.4. Analysis of corresponding MR imaging

Two experience orthopedic radiologists assessed to achieve

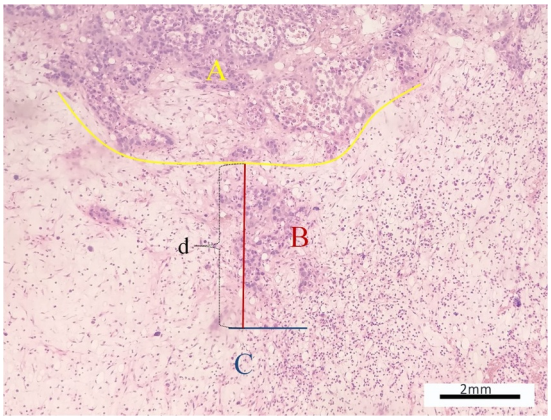

Fig. 2. (A,B) The two figures showed the distal ends of the tumor with micro-infiltration. Parenchyma area (A), micro-infiltration area (B) and simple edema area(C) were determined and the transition width defined by microscopy as the vertical distance (d) between the tumor margin to the most distal tumor cells on the marrow side and detected. (HE, ×100).

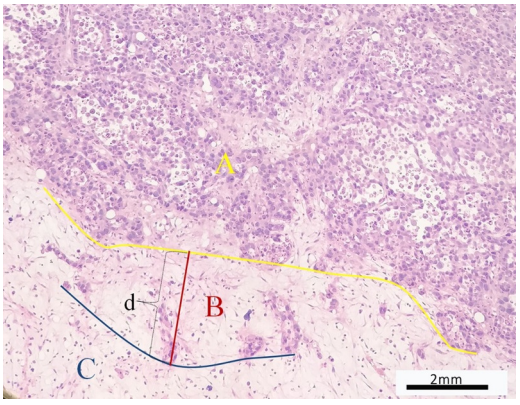

Fig. 2. (*continued*)

consensus with respect to the distal border of the tumor on T1WI, T2WI, and STIR sequences. The corresponding DCE images were analyzed by Extended Tofts linear model to obtain the quantitative parameters include *Ktrans, Kep,* v_e and v_p in parenchyma, micro-infiltration and simple edema area. Arterial input function (AIF) was obtained by measuring signal intensity changes in femoral artery. Three same size region of interests (ROIs) were identified in the parenchyma, micro-infiltration and simple edema areas respectively (Fig. 4). The voxel size of DCE image in x-y direction is 0.98 mm (right to left) × 0.84 mm (anteroposterior) and the area was about 0.8 mm^2 (0.98mm × 0.84 mm). The diameter of ROI is 3 mm and the area was about 7 mm^2. Each ROI include 8–9(7 mm^2/0.8 mm^2) voxels. In order to avoid the partial volume effect from one region into another, each ROI was placed three times, and the measured parameters were averaged.

2.5. Statistical analysis

One-way ANOVA was used to compare the differences between the parameters of the three areas, bilateral p values < 0.05 were thought to be significance. If significant differences were found between groups, the least significant difference (LSD) t-test was used to perform multiple comparisons. ROCs were plotted to determine the accuracy of different parameters by AUCs. Statistical analyses were performed with SPSS 19.0 version statistical software (IBM Corporation, Armonk, New York).

3. Results

Successful modeling was achieved in all 39 rabbits. Among them, 22 cases (22/39, 56.4%) had an infiltration boundary of tumor cell clusters embedded into the bone marrow and included into the micro-infiltration group. The depth of infiltration ranged from 1.3 mm to 4.6 mm, with an average depth of 3.2 mm ± 0.8 mm (Fig. 2). The other 17 cases were excluded from this research because their tumors showed a clear boundary under microscope.

All the 22 cases with infiltration boundaries showed isointensity in T1WI and hypointensity in both T2WI and STIR sequences. The bone marrow showed isointensity in T1WI and hyperintensity in both T2WI

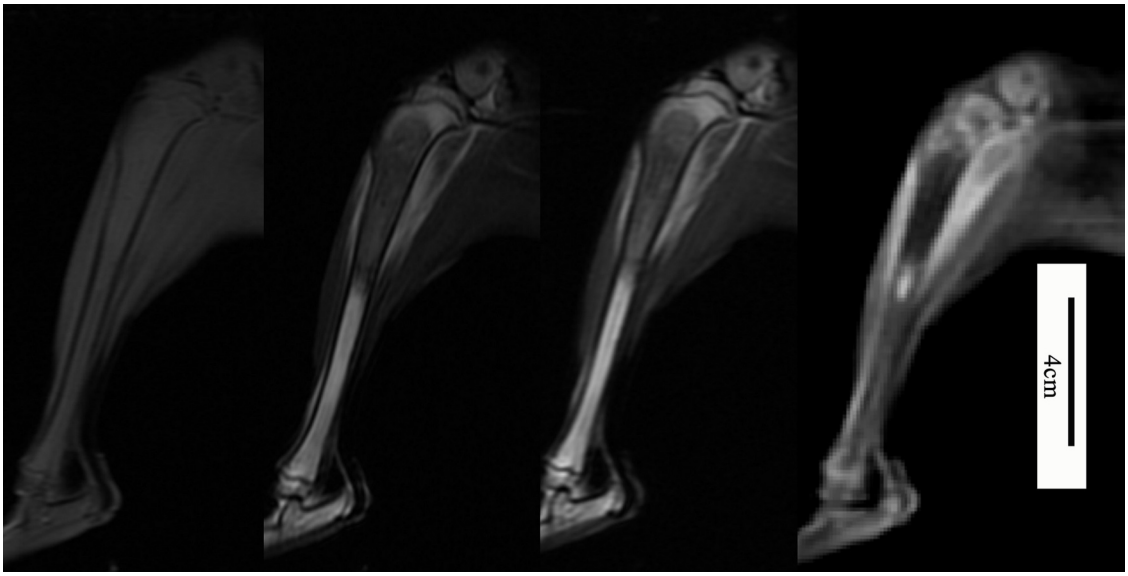

Fig. 3. The figures from left to right shows maximal sagittal sections of magnetic resonance image of T1WI, T2WI, short time inversion recovery (STIR) sequence and fast spoiled gradient echo (fast SPGR) sequence. The bone marrow shows isointensity in T1WI and hyper-intensity in both T2WI and STIR sequences because of the red marrow. The distal margins of the tumor were blurred in those sequences. (For interpretation of the references to color in this figure legend, the reader is referred to the web version of this article.)

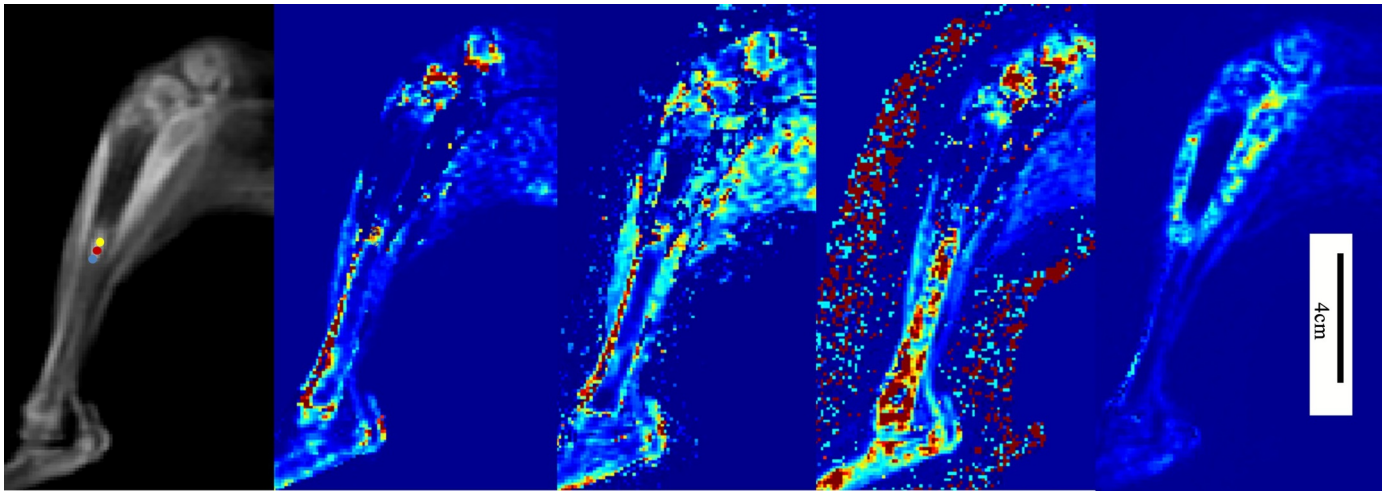

Fig. 4. The left figure showed original image of DCE-MRI. Parenchyma area (yellow dots), micro-infiltration area (red dots) and simple edema area (blue dots) were shown in the figure. The other four figures from left to right were pseudo-color images of quantitative parameters of *Ktrans, Kep,* v_e and v_p.

Table 1
Ktrans, Kep, ve and *vp* values (min $^{-1}$) in different areas.

Groups Parameters	parenchyma area	micro-infiltration area	simple edema area	F	*p*
Ktrans	0.494 ± 0.052	0.403 ± 0.049	0.173 ± 0.047	244.815	0.000
Kep	1.959 ± 0.65	1.528 ± 0.372	1.174 ± 0.486	12.756	0.000
ve	0.247 ± 0.068	0.283 ± 0.057	0.168 ± 0.062	19.406	0.000
vp	0.125 ± 0.036	0.108 ± 0.033	0.098 ± 0.025	4.037	0.022

and STIR sequences because of the red marrow. However, the distal margins of the tumor were blurred, so the conventional MRI could not be used to accurately judge the boundary and evaluate micro-infiltration area of the tumor (Fig. 3).

The statistical results of quantitative parameters (Fig. 4) in parenchyma area, micro-infiltration area and simple edema area were as follows: *ktrans* values were (0.494 ± 0.052), (0.403 ± 0.049), (0.173 ± 0.047) min^{-1} (p = =0.000), *kep* values were (1.959 ± 0.65), (1.528 ± 0.372), (1.174 ± 0.486) min^{-1} (p = =0.000), v_e values were (0.247 ± 0.068), (0.283 ± 0.057), (0.168 ± 0.062) min^{-1} (p = =0.000), v_p values were (0.125 ± 0.036), (0.108 ± 0.033), (0.098 ± 0.025) min^{-1} (p = =0.022), respectively(Table 1). Least significant difference (LSD) *t*-test was used to perform multiple comparisons between groups. *Ktrans* and *Kep* values had significant differences in the three areas, respectively. However, the v_p values between parenchyma area and micro-infiltration area (p = =0.078), micro-infiltration area and simple edema area (p = =0.315), and v_e values between parenchyma area and micro-infiltration area (p = =0.056) showed no significant differences (Fig. 5). v_e values were significant higher in parenchyma and micro-infiltration areas than the simple edema area.

ROCs were plotted to determine the accuracy of *ktrans* and *kep* by AUCs (Fig. 6). The results shows that *ktrans* has the highest accuracy in differentiating different areas (AUC = 0.948) and *kep* had moderate accuracy (AUC = 0.764) (Table 2).

4. Discussion

4.1. Pathophysiological characteristics of different regions

Tumor growth depends on angiogenesis. Tumor angiogenesis is quite different from physiological blood vessel formation. The morphological features of tumor angiogenesis include atypical branches of tumor vessels, incomplete endothelium and lack of functional smooth muscles, and high permeability in function [15]. In our study, the central region of the high-grade malignant bone tumor contained cystic degeneration and necrosis, whereas the peripheral region were mostly solid areas. Thus the surrounding solid area of the tumor can truly reflect the nature of the tumor.

Micro-structural change occurred earlier than morphologic changes [16]. Malignant bone tumors infiltrated into surrounding area in an unrestricted manner, with unclear boundaries, forming a micro-infiltration area that could not be detected by conventional imaging, and in which tumor growth was accompanied by tumor angiogenesis. A peri-tumoral interstitial reaction zone formed surrounding the tumor [17,18]. As shown in this study, tumor cells with large, irregular, and hyperchromatic nuclei were scattered in the background of normal bone marrow of this area, accompanied by an inflammatory cell infiltration and bone marrow edema. The micro-infiltration area lay between the parenchyma and simple edema areas, and there was significantly different blood perfusion, degree of vascularization and vascular permeability in the three areas.

4.2. Conventional MRI in evaluating intra-osseous tumor extension

Because of the high contrast between the hyper-intense fatty marrow and the intermediate-to-low signal of the tumor, non-contrast T1-weight spin echo sequence remains the gold standard to judge the extent of intramedullary infiltration of bone tumors [19,20]. However, several studies demonstrated that conventional MRI might overestimate or underestimate intra-osseous infiltration of the tumor [20]. In our study, the distal margins of the tumor were blurred. Two reasons can explain this result. First, malignant tumor infiltrated into surrounding area with an unclear boundary and showed unclear margin. Second, as malignant bone tumors are most common in teenagers, we selected immature rabbits with mainly red marrow that shows isointensity on T1WI for the study, and which led to decreased signal contrast between tumor and bone marrow. Hyper-intensity showed in T2WI and STIR sequences both in red marrow and the infiltration area, as well as the pure edema region.

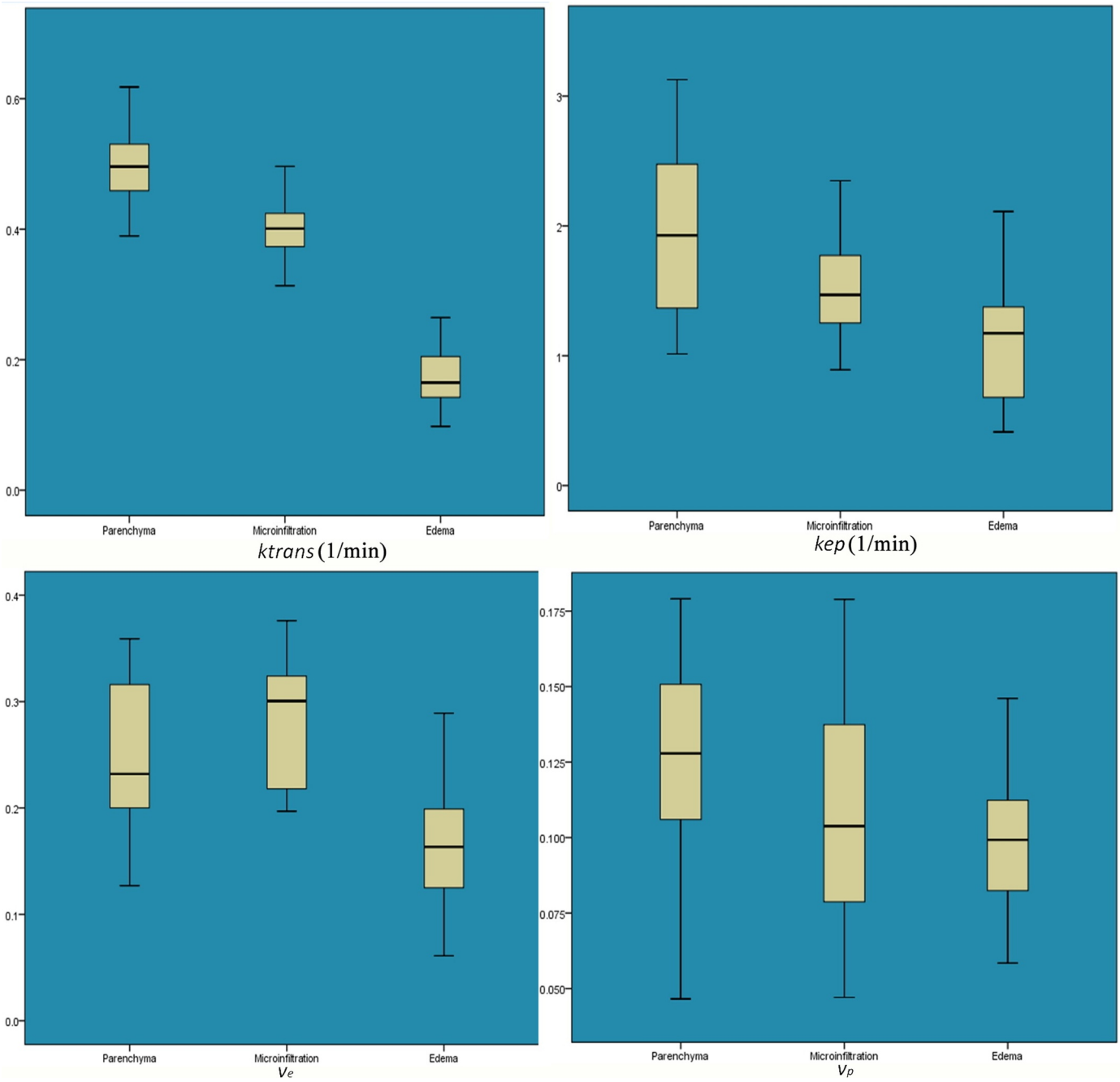

Fig. 5. Box-plots of the quantitative parameters. *Ktrans* and *Kep* were highest in the parenchyma area, intermediate in the micro-infiltration area and lowest in the simple edema area. The differences between the three regions were significant. v_e was higher in the parenchyma and micro-invasive areas than simple edema area. However, there were no significant differences in v_p and v_e values between parenchyma area and micro-infiltration area, v_p values between micro-infiltration area and simple edema area.

4.3. Role of DCE-MRI quantitative parameters in distinguishing different areas

DCE-MRI could evaluate spatial and temporal variations in tumor angiogenesis and predict biological aggressiveness and quantify blood flow, microvasculature, and capillary permeability in tumors [10,21]. Previous research showed the potential of quantitative parameters in assessing vascular effects to neoadjuvant chemotherapy in osteosarcoma and predicting event-free and overall survival in pediatric patients with osteosarcoma [22,23]. An extended Tofts linear model, which is a two compartment model that considers the intravascular extracellular volume fraction (blood plasma) to be the central compartment (v_p), and the extravascular-extracellular volume fraction (v_e) as the peripheral compartment, was used in our study to quantify the DCE-MRI data. The contrast agent introduced into the vasculature diffused into the extravascular-extracellular space in a reversible process characterized by a distribution rate constant (*Ktrans*) and a redistribution rate constant (*Kep*) [24,25]. The parameters *Ktrans, Kep,* v_e and v_p have been shown to reveal information about the micro-vascular environment of parenchyma area, micro-infiltration area and simple edema area.

No previous studies have used quantitative parameters of DCE-MRI to differentiate different regions of bone tumors. Yun et al. [26] applied quantitative parameters to differentiate true progression from pseudo-

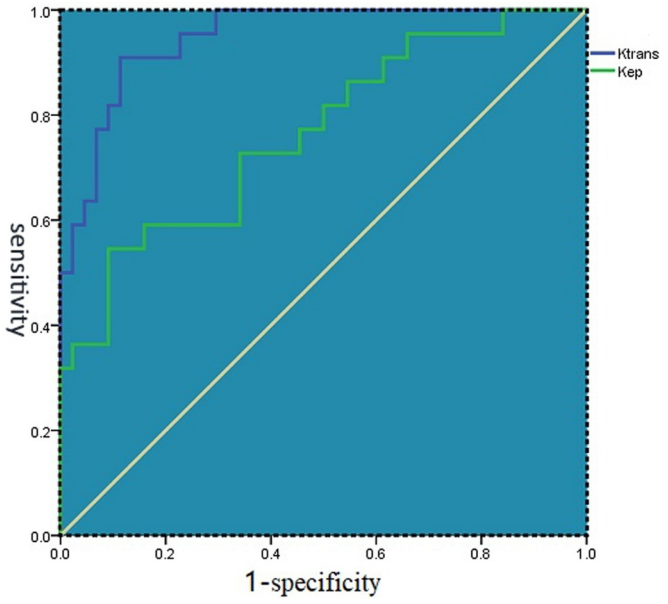

Fig. 6. ROCs of *Ktrans* and *Kep* shows that k*trans* had highest accuracy in differentiating different areas.

Table 2
AUCs of the ROCs of *Ktrans* and *Kep*.

Parameters	AUC
Ktrans	0.948
Kep	0.764

progression of glioblastoma after treated with concurrent radiation therapy and temozolomide chemotherapy; they found that mean *Ktrans* was higher in the true progression group than in the pseudo- progression group, and *Ktrans* was the only independently differentiating variable. Ocak et al. [27] found that *Ktrans* and *Kep* were significantly higher in cancer than in the normal peripheral zone in prostate cancer. The results in our study demonstrate that quantitative parameters *Ktrans* and *Kep* can be used to differentiate different areas within bone tumors, and *Ktrans* is the most accurate. The study by Lin et al. [28] drew similar conclusions that determination of *Ktrans* and *Kep* permit estimation of tumor angiogenesis and proliferation in human breast cancer. The values were highest in the parenchymal area, intermediate in the micro-infiltration area and loweset in the simple edema area. *Ktrans* is defined as the transfer rate of the contrast agent from blood plasma to extravascular extracellular space (EES) across the endothelial membrane, and represents a combination of blood flow, vascular permeability and microvessel density derived from the complex combination of these three factors [29]. *Kep* means the reflux of contrast agent from the EES to vasculature. Li et al. [30] found that *Kep* is mainly affected by microvascular permeability, and the value could more accurately reflect microvascular permeability in different regions. Actually, the parameters *Ktrans* and *Kep* represent a complex combination of variables like microvessel density, blood flow, and vascular permeability, so the observed differences in the three areas could result from one, two or even all of the factors and cannot distinguish the individual influence of these factors.

The parameter v_e means extra-vascular extracellular volume fraction. This study shows that v_e can not accurately distinguish the different regions, but can effectively distinguish the regions containing tumors cells from those without tumor cells. Therefore, v_e can be used to judge the infiltration range of tumors within the medullary space. The parameter is affected by many factors, such as the degree of cytogenesis, necrosis, leakage of contrast medium and reflux rate. The results show that v_e is higher in the parenchyma and micro-invasive areas. Because of the rich blood vessels and high permeability, the leakage of contrast medium is obviously more than that in the surrounding simple edema area. The study of Yun et al. [26] showed that v_e was higher in true progression than pseudo-progression and could be used to distinguish between the two in treated glioblastoma. The reason that v_e could not accurately distinguish between different regions may be because it is affected by so many factors. On one hand, the vascular permeability is higher in the parenchymal area than the micro-infiltration area. On the other hand, the tumor cell density is also higher in the parenchyma area.

The v_p is a measure of intravascular volume and a representation of tumor vascularity, a decline in v_p after radiation therapy of osseous spine metastasis probably represents the reduction in vascularity of a successfully treated lesion [31,32]. Our study shows that v_p cannot be used to distinguish the different regions and judge the actual infiltration range of tumors. The reason maybe that neovascularization occurred both in the tumor and inflammatory area. Similar to the results of this study, v_p played a limited role in evaluating the true and false progression of glioblastoma [26]. However, a significant difference in v_p between parenchyma area and simple edema area was shown, reflecting the of large amount of neovascularization within the parenchyma area.

4.4. Shortcomings of the present study

Firstly, imaging of quantitative parameters was not intuitive, and the sample size was relatively small to set boundary values for different regions; As a result, the findings of this study cannot yet be applied to clinical practice. Secondly, the relationships between the quantitative DCE-MRI parameters with VEGFR or MVD were not investigated, so the research cannot distinguish the influence of factors like microvessel density, blood flow, and vascular permeability on the parameters. Further immunohistochemistry studies would be needed to investigate further. Thirdly, quantitative parameters derived from the DCE-MRI data were sensitive to acquisition and post-processing techniques; this made it difficult to compare results obtained using the different methods. Issues of standardization, repeatability, reproducibility, and validation must be addressed in the future [25].

Conclusion

Quantitative parameters *Ktrans, Kep* and v_e can be used to assess the extent of intramedullary invasion of malignant bone tumors. *Ktrans* has the highest accuracy in differentiating different regions of bone tumors.

Funding sources

This work was supported by the National Natural Science Foundation of China [grant numbers 81571673, 81671658].

CRediT authorship contribution statement

Zhang Yuan: Writing - original draft, Writing - review & editing. **Tan Yiqing:** Validation, Formal analysis, Data curation. **Dong Cheng:** Investigation, Formal analysis. **Gao Sai:** Data curation. **Xu Wenjian:** Resources, Funding acquisition. **Chen Haisong:** Conceptualization, Methodology, Funding acquisition, Writing - review & editing.

Declaration of Competing Interest

The authors declare that there are no conflicts of interest.

Supplementary materials

Supplementary material associated with this article can be found, in

the online version, at doi:10.1016/j.jbo.2019.100269.

Reference

[1] H. Chen, M. Jia, W. Xu, Malignant bone tumor intramedullary invasion: evaluation with dual-energy computed tomography in a rabbit model.[j], J Comput. Assist. Tomogr. 39 (1) (2015) 70–74.

[2] H. Chen, Z. Wu, W. Xu, J. Pang, M. Jia, C. Dong, X. Li, Evaluating the scope of malignant bone tumor using ADC measurement on ADC map, Technol. Cancer Res. Treat. 18 (2018), https://doi.org/10.1177/1533033819853267 Jan-Dec1533033819853267.

[3] H. Chen, Y. Zhang, J. Pang, Z. Wu, M. Jia, Q. Dong, W. Xu, The differentiation of soft tissue infiltration and surrounding edema in an animal model of malignant bone tumor: evaluation by dual-energy ct, Technol. Cancer Res. Treat. 18 (2019), https://doi.org/10.1177/1533033819846842 Jan 11533033819846842.

[4] K. Lee F, A.D. King, B.B. Ma, et al., Dynamic contrast enhancement magnetic resonance imaging (DCE-MRI) for differential diagnosis in head and neck cancers[J], Eur. J. Radiol. 81 (4) (2012) 784–788.

[5] P. Sujlana, J. Skrok, M. Fayad L, Review of dynamic contrast-enhanced MRI: technical aspects and applications in the musculoskeletal system[J], J. Magn. Reson. Imaging 47 (4) (2018) 875–890.

[6] L.M. Fayad, M.A. Jacobs, X. Wang, J.A. Carrino, D.A. Bluemke, Musculoskeletal tumors: how to use anatomic, functional, and metabolic MR techniques, Radiology 265 (2012) 340–356.

[7] T.D. Coninck, L. Jans, G. Sys, et al., Dynamic contrast-enhanced MR imaging for differentiation between enchondroma and chondrosarcoma[J], Eur. Radiol. 23 (11) (2013) 3140–3152.

[8] M. Bollow, W. Knauf, A. Korfel, et al., Initial experience with dynamic MR imaging in evaluation of normal bone marrow versus malignant bone marrow infiltrations in humans, J. Magn. Reson. Imaging 7 (1) (1997) 241–250.

[9] L.A. Moulopoulos, T.G. Maris, N. Papnikolaou, et al., Detection of malignant bone marrow involvement with dynamic contrast-enhanced magnetic resonance imaging, Ann. Oncol. 14 (1) (2003) 152–158.

[10] H. Hawighorst, M. Libicher, M.V. Knopp, et al., Evaluation of angiogenesis and perfusion of bone marrow lesions: role of semiquantitative and quantitative dynamic MRI, J. Magn. Reson. Imaging 10 (3) (1999) 286–294.

[11] A. Stäbler, A. Baur, R. Bartl, et al., Contrast enhancement and quantitative signal analysis in MR imaging of multiple myeloma: assessment of focal and diffuse growth patterns in marrow correlated with biopsies and survival rates, AJR Am. J. Roentgenol. 167 (4) (1996) 1029–1036.

[12] A. Rhamouni, J.L. Montazel, M. Divine, et al., Bone marrow with diffuse tumor infiltration in patients with lymphoproliferative diseases: dynamic gadolinium-enhanced MR imaging, Radiology 229 (3) (2003) 710–717.

[13] Y. Zha, M. Li, J Yang, Dynamic contrast enhanced magnetic resonance imaging of diffuse spinal bone marrow infiltration in patients with hematological malignancies, Korean J. Radiol. 11 (2) (2010) 187–194 Mar-Apr.

[14] L. Zhang, C. Mandel, Z.Y. Yang, Q. Yang, R. Nibbs, D. Westerman, A Pitman, Tumor infiltration of bone marrow in patients with hemato-logical malignancies: dynamic contrast-enhanced magnetic resonance imaging, Chin. Med. J. (Engl.) 119 (15) (2006 Aug 5) 1256–1262.

[15] X.W. Bian, Q.L. Wang, H.L. Xiao, et al., Tumor microvascular architecture phenotype (T-MAP) as a new concept for studies of angiogenesis and oncology[J], J. Neurooncol. 80 (2) (2006) 211–213.

[16] D. Sidransky, M. Hollstein, Clinical implications of the p53 gene[J], Annu. Rev. Med. 47 (47) (1996) 285–301.

[17] S.J. Schnitt, Molecular biology of breast tumor progression: a view from the other side[j], Int. J. Surg. Pathol. 18 (3 Suppl) (2010) 170S–173S.

[18] G. Bierry, A. Venkatasamy, S. Kremer, J.C. Dosch, J.L Dietemann, Dual-energy CT in vertebral compression fractures: performance of visual and quantitative analysis for bone marrow edema demonstration with comparison to MRI, Skeletal Radiol. 43 (4) (2014) 485–492.

[19] G. Han, Y. Wang, W.Z. Bi, D.J. Wang, S.B. Lu, L. Zhang, B Zhao, Magnetic resonance imaging is appropriate for determining the osteotomy plane for appendicular osteosarcoma after neoadjuvant chemotherapy[J], Med. Oncol. 29 (2) (2012 Jun) 1347–1353.

[20] A. Saifuddin, B. Sharif, C. Gerrand, J Whelan, The current status of MRI in the preoperative assessment of intramedullary conventional appendicular osteosarcoma [J], Skeletal Radiol. 48 (4) (2019 Apr) 503–516.

[21] L.M. Fayad, C. Mugera, T. Soldatos, A. Flammang, F del Grande, Technical innovation in dynamic contrast-enhanced magnetic resonance imaging of musculoskeletal tumors: an MR angiographic sequence using a sparse k-space sampling strategy, Skeletal Radiol. 42 (2013) 993–1000.

[22] J. Guo, W.E. Reddick, J.O. Glass, et al., Dynamic contrast-enhanced magnetic resonance imaging as a prognostic factor in predicting event-free and overall survival in pediatric patients with osteosarcoma[J], Cancer 118 (15) (2012) 3776–3785.

[23] J. Guo, J.O. Glass, M.B. Mccarville, et al., Assessing vascular effects of adding bevacizumab to neoadjuvant chemotherapy in osteosarcoma using DCE-MRI[J], Br. J. Cancer 113 (9) (2015) 1282–1288.

[24] P.S. Tofts, G. Brix, D.L. Buckley, et al., Estimating kinetic parameters from dynamic contrast-enhanced T1-weighted MRI of a diffusable tracer: standardized quantities and symbols[J], J. Mag. Reson. Imaging 10 (3) (1999) 223–232.

[25] T.E. Yankeelov, J.C. Gore, Dynamic contrast enhanced magnetic resonance imaging in oncology: theory, data acquisition, analysis, and examples[j], Curr. Med. Imaging Rev. 3 (2) (2009 May 1) 91–107.

[26] T.J. Yun, C.K. Park, T.M. Kim, S.H. Lee, J.H. Kim, C.H. Sohn, S.H. Park, I.H. Kim, S.H. Choi, Glioblastoma treated with concurrent radiation therapy and temozolomide chemotherapy: differentiation of true progression from pseudoprogression with quantitative dynamic contrast-enhanced MR imaging[J], Radiology 274 (3) (2015) 830–840 Mar.

[27] L. Ocak, M. Bernardo, G. Metzger, et al., Dynamic contrast-enhanced MRI of prostate cancer a 3T: a study of pharmacokinetic parameters, AJR 189 (849) (2007) W192–W201.

[28] L. Lin, K. Wang, X. Sun, et al., Parameters of dynamic contrast-enhanced MRI as imaging markers for angiogenesis and proliferation in human breast cancer[j], Med. Sci. Monit. Int. Med. J. Exp. Clin. Res. 21 (2) (2015) 376–382.

[29] D.M. Yeo, S.N. Oh, C.K. Jung, et al., Correlation of dynamic contrast-enhanced MRI perfusion parameters with angiogenesis and biologic aggressiveness of rectal cancer: preliminary results[J], J. Magn. Reson. Imaging 41 (2) (2015) 474–480.

[30] X. Li, Y. Cai, B. Moloney, et al., Relative sensitivities of DCE-MRI pharmacokinetic parameters to arterial input function (AIF) scaling[J], J. Magn. Reson. 269 (2016) 104–112.

[31] S. Chu, S. Karimi, K.K. Peck, Y. Yamada, E. Lis, J. Lyo, M. Bilsky, A.I Holodny, Measurement of blood perfusion in spinal metastases with dynamic contrast-enhanced magnetic resonance imaging: evaluation of tumor response to radiation therapy, Spine (Phila Pa 1976) 38 (22) (2013) E1418–E1424 Oct 15.

[32] E. Lis, A. Saha, K.K. Peck, J. Zatcky, M.J. Zelefsky, Y. Yamada, A.I. Holodny, M.H. Bilsky, S Karimi, Dynamic contrast-enhanced magnetic resonance imaging of osseous spine metastasis before and 1 h after high-dose image-guided radiation therapy, Neurosurg. Focus 42 (1) (2017 Jan) E9.